

NONLINEAR OPTICAL PHENOMENA https://doi.org/10.1070/QEL16923

Study of nonlinear optical properties of TiO_2–polystyrene nanocomposite films

M. Zeinali, B. Jaleh, M.R. Rashidian Vaziri, A. Omidvar

Abstract. **We consider an *ex-situ* prepared TiO_2–polystyrene (TiO_2–PS) nanocomposite, with different concentration of TiO_2 nanoparticles (NPs), deposited by the spin-coating method on quartz substrates. Nonlinear optical properties of the TiO_2–PS nanocomposite films are studied using the *Z*-scan technique. Structural properties of the films are investigated using scanning electron microscopy (SEM) and X-ray diffraction (XRD) measurements. The optical band gap energy of the TiO_2–PS films are determined from the optical absorption spectra. The relation between the optical nonlinearities and the bandgap energy, as a microscopic electronic property of the semiconductor nanocomposite, is established. It is shown that an increase in the content of TiO_2 NPs in the nanocomposite films results in bandgap narrowing and concomitant enhancement of optical nonlinearities. It is proposed that bandgap narrowing and enhancement of optical nonlinearities can be ascribed to the introduction of mid-gap states as a result of the formation of surface defects in TiO_2 NPs. The results of this work indicate that incorporation of TiO_2 NPs in the PS polymeric matrix can be a new way for bandgap narrowing of TiO_2 NPs toward the visible light region, which is of great interest for their application in this part of the spectrum. Furthermore, enhancement of the optical nonlinearities of the spin-coated TiO_2–PS films by increasing the TiO_2 NP content can open up new avenues for their use as nonlinear optical films in photonics applications.**

Keywords: *nanostructures, thin films, optical properties, photonics applications.*

1. Introduction

Recently, synthesis of polymeric matrices embedded with semiconductor nanoparticles (NPs) has attracted much interest in the field of nanomaterials [1]. Semiconductor NPs have been investigated extensively due to their promising applications in optoelectronics and photonics [2]. Specifically, oxide semiconductor NPs are currently being studied widely, considering their tunable electronic and optical properties and the potential applications in many areas, such as field emission displays, solar cells, light-emitting diodes, optical switches and gas sensors [3]. The effects of concentration and wide band gap semiconductor NPs in polymer matrices have attracted increasing attention because of their tunable optical properties and importance in science and technology [4]. In polymer nanocomposites, polymer chains not only stabilise the NPs but also act as linkers and help achieve an extended framework of NPs in a polymer matrix [5].

Among oxide semiconductor NPs, TiO_2 NPs are elaborately studied because of their promising applications in different fields such as photovoltaics, photoelectronics and sensors [6]. TiO_2 polymer nanocomposite films have also attracted much interest in recent years because of their tunable physical properties [7]. As a low specific weight polymer, polystyrene (PS) is of interest because of its mechanical flexibility and high chemical resistance [8]. Many research efforts have been focused on synthesis of high-quality, transparent films including TiO_2 polymer nanocomposites and on investigating their optical properties [9]. Nonlinear optical properties of such materials have also received great attention [10–13]. Large reverse saturable absorption, increase in the optical absorbance with increasing power of the incident light, has been reported in poly(styrene–maleic anhydride)/TiO_2 nanocomposite [10]; however, the nonlinear refractive index of these nonacomposites has not been studied in this paper. Furthermore, an increase in the nonlinear refractive index and absorption coefficient has been reported for TiO_2 nanorods/PMMA copolymer-based [11] and poly(methylmethacrylate)/TiO_2 nanocomposites [12]. Despite the fact that TiO_2 polymer nanocomposite films have been studied for a long time, little work has been done in terms of realising active nonlinear optical devices using these materials. Indeed, before they can be practically used in these types of devices, their nonlinear optical properties must be further enhanced.

Nonlinear optical thin films are very attractive for a number of information processing and photonics applications, like optical switches, high speed electro-optic modulators, integrated optics components and optical waveguides for frequency conversion by low-power semiconductor lasers [14, 15]. As is already indicated [16], for such applications the film thickness must be of the order of $\sim$1 μm and it must have good optical quality over large dimensions, on the order of centimeters. Spin-coating is one of the most common techniques for uniformly depositing nanocomposite solutions over large-area substrates to prepare high quality thin films for technological applications [17]. By varying the spin speed in this technique, films with a thickness ranging from a few nanometres to a few micrometers can be prepared. Hence, spin-coating can be fruitfully used as the method for preparing nonlinear optical thin films from nanocomposite solutions.

M. Zeinali, B. Jaleh, A. Omidvar Department of Physics, Bu-Ali Sina University, P.O. Box 65174, Hamedan, Iran;
M.R. Rashidian Vaziri Photonics and Quantum Technologies Research School, Nuclear Science & Technology Research Institute, Tehran, Iran; e-mail: rezaeerv@gmail.com

Received 3 December 2018; revision received 21 April 2019
Kvantovaya Elektronika **49** (10) 951–957 (2019)
Submitted in English

Semiconductors are attractive nonlinear optical materials because of their large nonlinearities and fast response times to the exciting light. Measuring the optical nonlinearity of these materials and determining its dependence on microscopic electronic material properties, like the band gap energy, can be very promising for practical applications [18]. The obtained tabulated data not only allow one to select a material with large nonlinearity for a specific application but also to predict the specific material parameters that determine these high nonlinearities. When one searches for a highly nonlinear material, this predictive capability is quite crucial [18]. A number of experimental studies have investigated the relation between the optical nonlinearities and microscopic electronic properties of semiconducting materials [18–21]. However, because of the rapidly growing field of semiconductors, further investigation concerning the determination of the dependence of nonlinear optical properties of the newly developed semiconducting materials on their microscopic electronic properties seems urgent.

Various approaches have been reported for the preparation of NPs/polymer composites. As is well-known, there are two basic techniques for preparing NPs/polymer composites: *in-situ* and *ex-situ* techniques [22]. In the *in-situ* technique, NPs are generated in the presence of a polymer, and in the *ex-situ* technique, separately prepared NPs are added to the polymer matrix. Compared with the *in-situ* technique, the *ex-situ* technique provides a better control over the amount of NPs loading in the polymer matrix. For the NPs/polymer composites prepared in the solution, spin-coating is one of the easiest methods to deposit them as thin films on various supports [23].

In this work, we report the preparation of TiO_2–PS nanocomposite using an *ex-situ* technique and deposition of nonlinear optical thin films from this nanocomposite, with different percentages of the TiO_2 NPs (2%, 4% and 6%) by the spin-coating method. Nonlinear optical properties of the TiO_2–PS nanocomposite films have been studied using the *Z*-scan technique. It is shown that an increase in the content of TiO_2 NPs in the PS films is a novel way for bandgap narrowing of TiO_2 NPs toward the visible light region and concomitant enhancement of nonlinear optical properties of the TiO_2–PS films. Bandgap narrowing of TiO_2 NPs toward the visible light region facilitates the development of photonic devices with these types of NPs for their favorable application in this part of the spectrum. Furthermore, enhancement of the optical nonlinearities of the spin-coated TiO_2–PS films by increasing the content of TiO_2 NPs can open up new avenues for their use as nonlinear optical films in photonics applications.

2. Experimental

2.1. Instruments and reagents

High-purity chemical reagents were purchased from the Merck and Aldrich chemical companies. All materials were of commercial reagent grade. Titanium dioxide powder (Degussa, P-25), polystyrene and toluene were used to prepare nanocomposites.

X-ray diffraction (XRD) measurements were performed using a Philips powder diffractometer type PW 1373 goniometer (Cu Kα λ = 1.5406 Å). The scanning rate was 2 degrees per minute in the 2-hour range from 10 to 50 degrees. UV–visible extinction spectra were recorded on a double beam PerkinElmer 550ES spectrophotometer with a resolution of 1 nm. Particle morphology and dispersion were investigated by a JEOL 4000-EX scanning electron microscope (SEM). Thickness measurements of the prepared films were performed using a Veeco Dektak-3 profilometer. Using a pulsed Nd:YAG laser (1064 nm, pulse length of 12 ns), the laser induced damage threshold of the thin films was measured in the '1- on-1' regime according to ISO 11254-1.

2.2. Preparation of nanocomposite films

The TiO_2–PS nanocomposite thin films were prepared using the spin-coating method. First, the PS was dissolved in toluene in 3 wt.% (2 g of PS & 65 g of toluene). Then, TiO_2 NPs were added to the solution with different percentages of 2%, 4% and 6% (0.04 g, 0.08 g and 0.12 g, respectively). The resulting colloidal solution was vigorously stirred ultrasonically for 15 min to achieve homogeneous dispersion of TiO_2 NPs in the PS matrices. The solution was spin-coated on quartz substrates at 2000 rpm for 2 min and cured at 70 °C for 30 min in a vacuum oven. The quartz substrates were carefully cleaned prior to film deposition by putting them in chromic acid for 20 min and subsequent ultrasonication in acetone and deionised water for several times. For the sake of brevity, the nanocomposite films obtained from different percentages of 2%, 4% and 6% of the TiO_2 NPs will be respectively named as PS–2%TiO_2, PS–4%TiO_2 and PS–6%TiO_2. For comparison with the nanocomposite films, the films were also deposited from the prepared PS solution in the first step, with exactly the same deposition conditions, which will be referred to as the pure PS films.

2.3. *Z*-scan measurements

The nonlinear absorption coefficient and the nonlinear refractive index of all the prepared films were measured using the *Z*-scan technique. The schematic of the used *Z*-scan experimental setup is shown in Fig. 1. A cw He–Ne laser (Melles Griot, 50 mW, 632.8 nm) was used as a pump source. The laser beam was divided by a beam splitter (BS) and directed in two different paths of the optical setup. One half of the original laser beam, as the reference beam, was directed toward the first power meter (PM1). Another one-half of the beam, as the signal beam, was focused to a spot of size 22 μm by a convex lens (L) with a focal length f = 20 cm and then passed through the thin film. The laser beam spot size was deter-

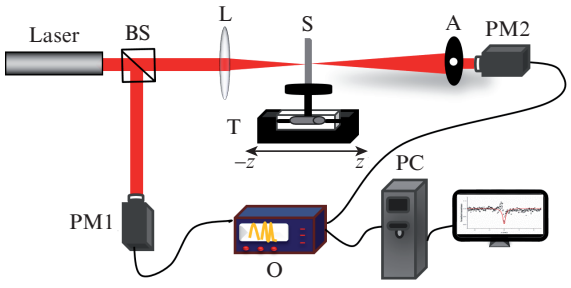

Figure 1. Schematic of the *Z*-scan measurement optical setup: (BS) beam splitter; (L) focusing lens; (S) thin-film sample; (T) translation stage; (A) aperture; (PM1, PM2) power meters; (PC) personal computer; (O) oscilloscope.

mined by the scanning knife-edge method. The cell with the film sample was moved along the optical z axis from one to the other side of the lens focal point. In closed-aperture Z-scan measurements, the real part of the nonlinear refractive index was measured by recording and analysing the measured signal by the second power meter (PM2) after the beam passed through a far-field aperture (A). An aperture with the diameter of 1.5 mm, which lies in the desirable aperture diameter range for closed-aperture Z-scanning [24], was used in the measurements. Since the material acts as a weak z-dependant lens at high laser beam intensities [25], the aperture makes it possible to detect the small beam distortions in the original beam.

In open-aperture Z-scan measurements, the imaginary part of the nonlinear refractive index was measured by removing the aperture and measuring the whole signal by the power meter. In this way, small beam distortions due to the action of the real part of the nonlinear refractive index become insignificant and the beam power variations is due to the effect of the imaginary part, i.e. the nonlinear absorption coefficient [26]. In closed- and open-aperture measurements, the signal beam power was divided to the reference beam power at each z position to obtain the normalised transmittances T_{closed} and T_{open}.

3. Results and discussion

Figure 2 shows the optical extinction spectrum of TiO_2 NP dispersion in water and the extinction spectra of the pure PS, PS–2% TiO_2, PS–4% TiO_2 and PS–6% TiO_2 films. One can see that TiO_2 NPs highly absorb the light in the UV range. The absorption peak of pure TiO_2 is located around 324 nm, in good agreement with the previously reported locations for the absorption peaks of TiO_2 NPs in anatase crystalline phase [27, 28]. As is well-known, in nanocomposite materials, absorption and scattering of light from the nanosized structures both contribute to the extinction, and hence the extinction cross section σ_{ext} can be written as [29, 30]:

$$\sigma_{ext} = \sigma_{abs} + \sigma_{sca}, \quad (1)$$

where σ_{abs} and σ_{sca} are, respectively, the absorption and the scattering cross sections. Hence an increase in extinction with increasing percentage of TiO_2 NPs in nanocomposite films can be ascribed to the more intense light scattering from NPs. A more or less monotonic increase in the extinction for the entire optical extinction measurement range indicates that the scattering cross section of TiO_2 NPs is not highly wavelength-dependent.

The measured damage threshold of the films is presented in Table 1. The measured values indicate that with increasing content of TiO_2 NPs in nanocomposite films their damage threshold slightly decreases. This is consistent with the optical absorption data in Fig. 2b that indicate higher extinctions with increasing NP content in the films.

Table 1. The measured damage threshold of thin nanocomposite films.

Sample	Damage threshold/J cm^{-2}
PS–2%TiO_2	7.31 ± 0.11
PS–4%TiO_2	7.11 ± 0.21
PS–6%TiO_2	6.87 ± 0.10

The linear optical absorption coefficient of TiO_2 nanocomposites near their band edge can be expressed as [27]:

$$\alpha_0 h\nu = A(h\nu - E_g)^{1/2}, \quad (2)$$

where E_g is the band gap energy, A is a constant, and $h\nu$ is the photon energy. The band gap energies can be estimated by extrapolating the linear regions in plots of $(\alpha_0 h\nu)^2$ versus the photon energy (see Fig. 3). The band gap energies of the samples are listed in Table 2. The estimated value of the band gap

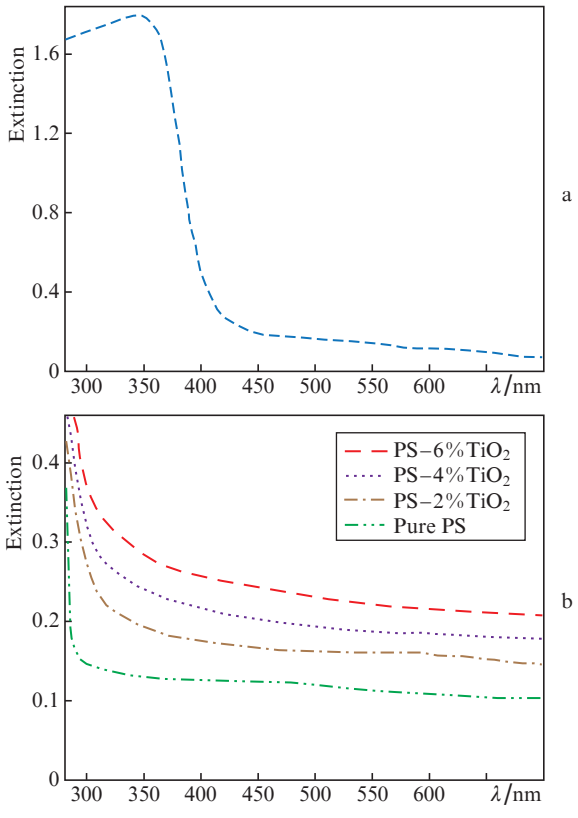

Figure 2. Measured optical extinction spectra of (a) TiO_2 NPs in water and (b) pure PS, PS–2%TiO_2, PS–4%TiO_2 and PS–6%TiO_2 thin films.

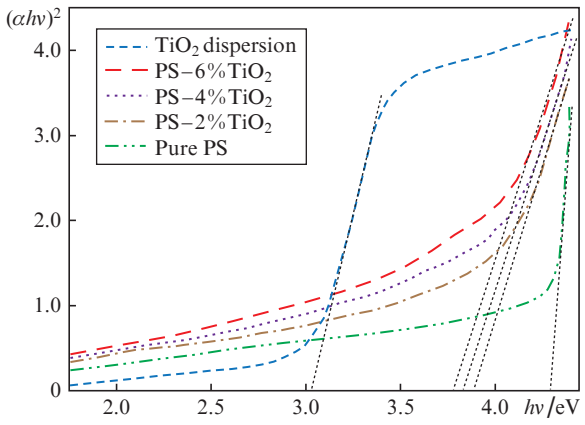

Figure 3. Estimation of the band gaps by extrapolation of the linear parts of the plots to $\alpha = 0$.

energy for the dispersion of TiO_2 NPs in water is very close to the reported band gap values for the bulk TiO_2 (~3.2 eV for anatase phase [27]). The difference can be explained by the fact that the band gap of TiO_2 and other semiconductor NPs is found to be size dependent due to the quantum size effect [31]. Furthermore, the water environment may also change the electrical properties of NPs [32].

Table 2. The estimated optical band gap energies of TiO_2 dispersion and TiO_2 nanocomposites. The mean values are calculated by averaging over the band gap energies obtained from all the prepared samples (8 samples in each case).

Sample	E_g/eV
TiO_2 dispersion in water	3.03 ± 0.02
PS–2%TiO_2	3.89 ± 0.01
PS–4%TiO_2	3.83 ± 0.01
PS–6%TiO_2	3.78 ± 0.02

Another noteworthy point in Fig. 3 is that by increasing the amount of TiO_2 NPs in nanocomposite films, their band gap red-shifts toward the visible light region. Band gap narrowing of TiO_2 NPs is of great interest to shift their absorption edge toward the visible region [33–35]. Previous studies indicated the dominant role of surface disorders [35] and point defects, like oxygen vacancies [36] and titanium interstitials [37] in controlling the band gap narrowing in this material. Band gap narrowing in our PS–TiO_2 nanocomposite films can also be ascribed to the introduction of surface disorders in TiO_2 NPs by the PS matrix, which increases with increasing number of TiO_2 NPs. As is already reported [35], hydrogenation of TiO_2 NPs can also produce a disordered layer on the surface of the NPs and decrease their band gap energy.

The structural information about the TiO_2 NPs, PS, and PS–6% TiO_2 films was analysed by XRD measurements (Fig. 4). The XRD spectrum of the TiO_2 NPs [Fig. 4, curve (*1*)] demonstrates that their major crystalline phase is anatase, as evidenced by the peaks at $2\theta = 25.3°$, 37.8° and 48.1°, consistent with the standard XRD data (JCPDS 21-1272). The weaker peak at $2\theta = 27.4°$ also indicates the presence of a minor rutile phase (JCPDS 21-1276) [38]. The phase contents of TiO_2 NPs were calculated using the equation [39]:

$$f = \frac{1}{1 + 1.265(I_R/I_A)}, \quad (3)$$

where I_A and I_R are, respectively, the integrated intensity of anatase and rutile peaks; and f is the weight fraction of the anatase phase in the TiO_2 compound. The phase percentages of anatase and rutile were obtained to be 81% and 19%, respectively. These results are consistent with previous reports that anatase is the major phase in TiO_2 photocatalyst (Degussa, P-25) [40]. The absence of sharp Bragg peaks and a large bump in a wide 2θ range clearly suggest the amorphous nature of the PS films [Fig. 4, curve (*2*)]. In the PS–6%TiO_2 film [Fig. 4, curve (*3*)], the intensity of both anatase and rutile peaks are influenced in the presence of PS. The intensity decrease of the crystalline phases in the PS–6%TiO_2 film partly confirms the band gap narrowing due to introduction of surface disorders in NPs by the PS matrix.

Cross-sectional SEM/EDS analysis of the PS–6%TiO_2 nanocomposite film in Fig. 5 shows that films with uniformly embedded TiO_2 NPs were indeed made by the spin-coating process. Chemical interaction between the surface of TiO_2 NPs and the PS polymer surrounding may introduce structural surface defects and alter the semiconducting properties of the nanocomposite films [41]. This can be confirmed by the XRD patterns in Fig. 4 and the calculated band gap values (Table 2).

The recorded open- and closed-aperture Z-scan signals for PS–2%TiO_2, PS–4% TiO_2 and PS–6%TiO_2 films are, respectively, shown in Figs 6 and 7. The fitting curves based on using the Z-scan theory [42] are also shown by solid lines. Nonlinear absorption coefficients β are deduced by performing a one-parameter fit on the open-aperture Z-scan signal, using the relation:

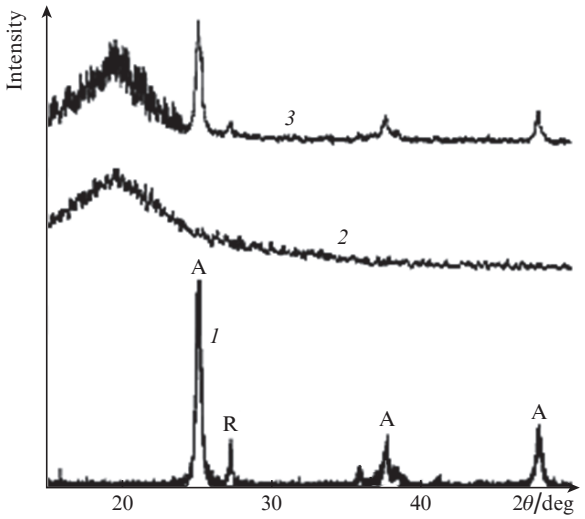

Figure 4. XRD patterns of (*1*) TiO_2 NPs, (*2*) PS film and (*3*) PS–6% TiO_2 nanocomposite film. A and R stand for the anatase and rutile phases, respectively.

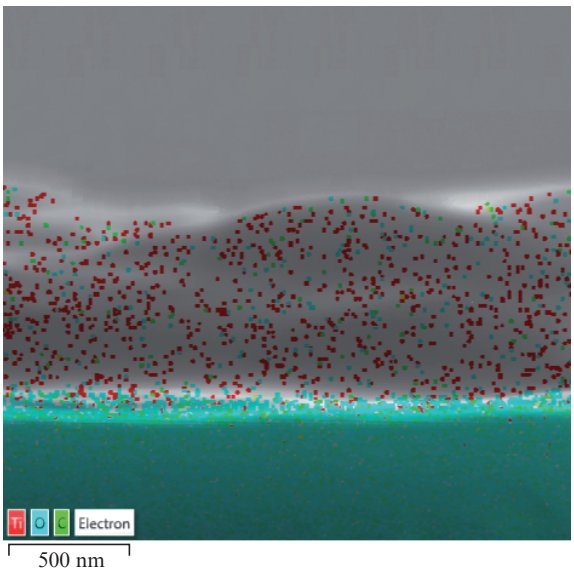

Figure 5. Cross-sectional SEM/EDS analysis of the PS–6%TiO_2 nanocomposite film.

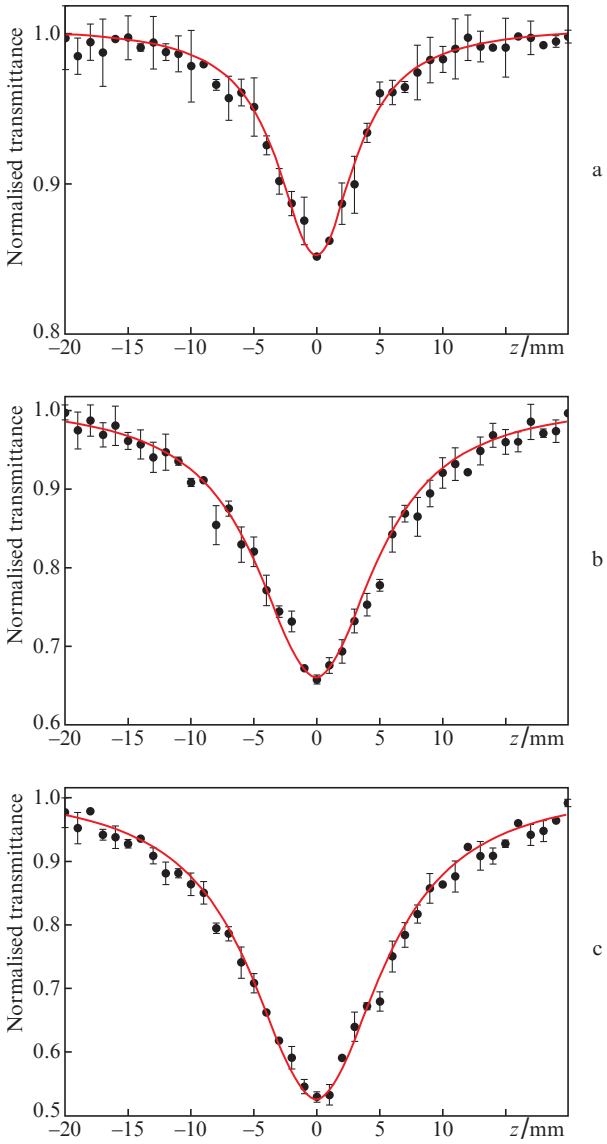

Figure 6. Open-aperture Z-scan signals (dots) and fitting results (solid lines) of (a) PS–2%TiO_2, (b) PS–4%TiO_2 and (c) PS–6%TiO_2 nanocomposite films.

$$T_{\text{open}}(z) = \frac{\ln[1 + q_0(x)]}{q_0(x)}, \tag{4}$$

where

$$q_0(x) = \frac{\beta I_0 d_{\text{eff}}}{1 + x^2}; \tag{5}$$

$x = z/z_0$; $d_{\text{eff}} = [1 - \exp(-\alpha_0 d)]/\alpha_0$ is the effective thickness, which is defined using the sample real thickness d and linear absorption coefficient α_0; I_0 is the on-axis intensity at the lens focus; and z_0 is the Rayleigh length of the laser beam.

Nonlinear refractive indices n_2 are also obtained by fitting the nonlinear transmission equation on the closed-aperture Z-scan signals [43]:

$$T_{\text{closed}}(z) = 1 - \frac{[4kn_2x + \beta(x^2 + 3)]I_0 d_{\text{eff}}}{(x^2 + 9)(x^2 + 1)}, \tag{6}$$

where k is the wave number. Nonlinear least squares fitting of the MATLAB environment is used to fit equations (4) and (6) on the measured open- and closed-aperture Z-scan signals, respectively. The deduced nonlinear optical constants of the nonocomposite films are summarised in Table 3. The reported standard deviation values for the nonlinear quantities have been obtained by using six identically prepared films and repeating the Z-scan measurements on five randomly selected points over the whole surface of each film.

Table 3. The nonlinear optical constants n_2 и β of nanocomposite films from the Z-scan; d is the measured thickness of the films.

Sample	$n_2/10^{-12}$ m^2 W^{-1}	$\beta/10^{-5}$ m W^{-1}	d/μm
PS–2%TiO_2	1.14 ± 0.13	0.69 ± 0.18	1.06 ± 0.22
PS–4%TiO_2	8.22 ± 0.16	2.45 ± 0.12	1.09 ± 0.13
PS–6%TiO_2	14.43 ± 0.10	3.76 ± 0.08	1.05 ± 0.20

The positive values of the nonlinear absorption coefficient β are consistent with the discernible valleys in open-aperture Z-scan signals in Fig. 6 and indicate the reverse saturable absorption in the samples, which, as it is reported in some papers [12, 44, 45], is characteristic of the TiO_2 nanocomposites. The positive values of the nonlinear refractive index n_2 are also consistent with the observable valley–peak sequential structures in Fig. 7, which also determine the nonlinear response of TiO_2 nanocomposites [44, 45]. The most noteworthy point about the encapsulated data in Table 3 is that an increase in the content of TiO_2 NPs in the films leads to the concomitant enhancement in their nonlinear optical properties. Enhancement of the nonlinear optical properties can also be discerned by noting that in Figs 6 and 7, deeper valleys and larger peak-to-valley transmittance differences are obtained by increasing the TiO_2 NP content in the films [46].

At this point, it would be useful to estimate the effect of the laser power on the thin films. Indeed, under high intensity illumination, a nonlinear Kerr medium reacts like a weak z-dependent lens during the Z-scan measurements. The focusing power of this weak nonlinear lens depends on the laser power and the physical constants of the medium [25]:

$$f_{\text{eff}}(z) = \frac{a\pi w^4(z)}{8n_2 P d_{\text{eff}}}, \tag{7}$$

where a is a correction factor ($3.77 < a < 6.4$) that accounts for the omitted higher order terms in the Taylor series expansion of the exponential of the nonlinear phase shift, and $w(z) = w_0\sqrt{1 + (z/z_0)^2}$ is the laser beam radius at a distance z from the waist [25]. Assuming a typical value of 5 for a, the focusing power of the nonlinear lens at $z = 0$ (corresponding to the focal point of the used convex lens in the Z-scan experimental setup, see Fig. 1) will be equal to 7.61, 1.03 and 0.61 m for PS–2%TiO_2, PS–4%TiO_2 and PS–6%TiO_2 films, respectively. Hence, by increasing the TiO_2 content of the films, stronger nonlinear lenses will be formed and, as evidenced by Fig. 7, stronger Z-scan signals will be generated.

Dependences of optical nonlinearities of the nanocomposite materials on their band gap energy are shown in Fig. 8. Band gap narrowing and enhancement of optical nonlinearities by increasing the content of NPs, are both clearly observed. One must note that this figure clearly demonstrates that the observable increase in the optical absorbance by

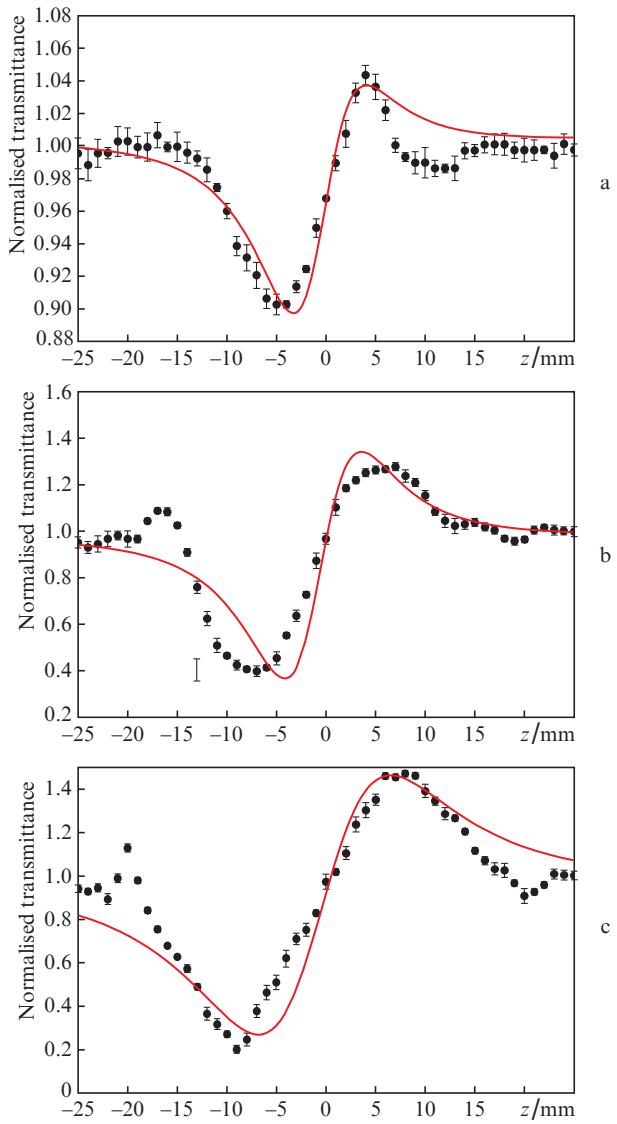

Figure 7. Closed-aperture *Z*-scan signals (dots) and fitting results (solid lines) of (a) PS–2%TiO_2, (b) PS–4%TiO_2 and (c) PS–6%TiO_2 nanocomposite films.

increasing the light intensity (Fig. 6) is due to single photon reverse saturable absorption in these films. Considering the energy of the incident light photons on these materials (1.96 eV), which corresponds to a wavelength of ~632.8 nm, the probability of two-photon absorption decreases by moving away from the required energy for this process (3.92 eV). Hence, the observable enhancement of nonlinear absorption by increasing the content of TiO_2 NPs in PS–TiO_2 nanocomposite films is due to single-photon reverse saturable absorption [47].

As we already pointed out, the PS matrix can produce different types of surface defects in TiO_2 NPs and reduce the band gap energy. We are of the opinion that the enhancement of optical nonlinearities by increasing the content of NPs in PS–TiO_2 nanocomposite films can also be ascribed to the appearance of surface defects in TiO_2 NPs by the PS matrix. As was already reported, defects and disorders can cause the band gap narrowing of TiO_2 by introducing the mid-gap states in this material [35–37]. Oxygen vacancies introduce vacancy states with energies from 0.75 to 1.18 eV below the conduction band minimum of TiO_2 [36], which supports our nonlinear absorption measurement results that show the enhancement of nonlinear absorption coefficient of PS–TiO_2 films by incorporation of a larger number of TiO_2 NPs. By increasing the content of NPs in these films, the density of defect states also increases in the mid-gap of TiO_2, which facilitates the single photon reverse saturable absorption process. The possibility of mid-gap state creation in PS–TiO_2 nanocomposite by different types of surface defects, like oxygen vacancies, must be further investigated in future studies, for instance by first-principles density functional theory (DFT) calculations, to be able to concretely explain about the role of defects in the enhancement of optical nonlinearites of this material.

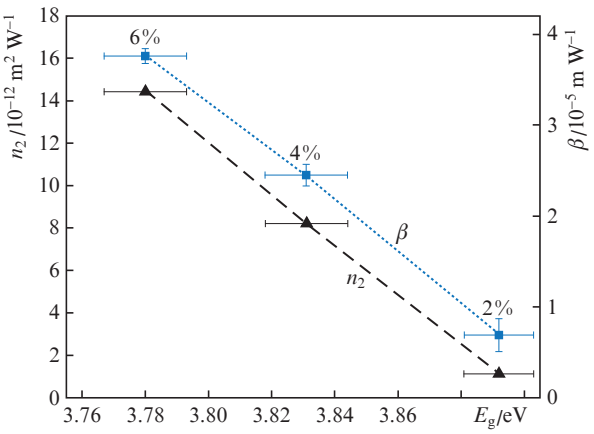

Figure 8. Dependences of optical nonlinearities of the nanocomposite films on their band gap energies; 2%, 4% and 6% stand for PS–2%TiO_2, PS–4%TiO_2 and PS–6%TiO_2 nanocomposite films, respectively.

4. Conclusions

The TiO_2–PS nanocomposite films have been prepared by the spin-coating method and the effect of the concentration of TiO_2 NPs on their optical properties has been studied. It has been shown that the optical band gap energy of the nanocomposite films decreases with increasing content of the TiO_2 NPs while their optical nonlinearities increase. It has been found that the TiO_2–PS nanocomposite films show self-defocusing nonlinearity as well as reverse saturable absorption behaviour. The results of this work indicate that incorporation of TiO_2 NPs in the PS polymeric matrix can be a new way for band gap narrowing of TiO_2 NPs toward the visible light region, which is of great interest for their application in this part of the spectrum [33–35]. Furthermore, enhancement of the optical nonlinearities of the spin-coated TiO_2–PS films by increasing the TiO_2 NP content can open up new avenues for their use as nonlinear optical films for a number of photonics applications [14, 16].

As is proposed in this paper, enhancement of optical nonlinearities by increasing the content of NPs in TiO_2–PS nanocomposite films can be ascribed to the generation of surface defects in TiO_2 NPs by the PS matrix. In order to more clearly confirm the role of surface defects, the possibility of mid-gap state generation in PS–TiO_2 nanocomposite by different types of surface defects can be further investigated in future studies, for instance by first-principles density functional theory (DFT) calculations [37]. The relation between band gap

narrowing and enhancement of optical nonlinearities can also be further investigated in future studies for other types of newly developed semiconducting materials.

References

1. Dilag J., Kobus H., Ellis A.V. *Forensic Sci. Internat.*, **228**, 105 (2013).
2. Tripathi S., Sharma M. *Mater. Res. Bull.*, **48**, 1837 (2013).
3. Corcoran B., Monat C., Grillet C., Moss D.J., Eggleton B.J., White T., O'Faolain L., Krauss T.F. *Nat. Photonics*, **3**, 206 (2009).
4. Wang Z.L., Song J. *Science*, **312**, 242 (2006).
5. Bala V., Sharma M., Tripathi S., Kumar R. *Mater. Chem. Phys.*, **146**, 523 (2014).
6. Chen X., Mao S.S. *Chem. Rev.*, **107**, 2891 (2007).
7. Xu Q.F., Liu Y., Lin F.-J., Mondal B., Lyons A.M. *ACS Appl. Mater. Interfaces*, **5**, 8915 (2013).
8. Zan L., Tian L., Liu Z., Peng Z.A. *Appl. Catal. A: General*, **264**, 237 (2004).
9. Chau J.L.H., Tung C.-T., Lin Y.-M., Li A.-K. *Mater. Lett.*, **62**, 3416 (2008).
10. Wang S., Zhang L., Su H., Zhang Z., Li G., Meng G., Zhang J., Wang Y., Fan J., Gao T. *Phys. Lett. A*, **281**, 59 (2001).
11. Sciancalepore C., Cassano T., Curri M., Mecerreyes D., Valentini A., Agostiano A., Tommasi R., Striccoli M. *Nanotechnol.*, **19**, 205705 (2008).
12. Elim H., Ji W., Yuwono A., Xue J., Wang J. *Appl. Phys. Lett.*, **82** 2691 (2003).
13. Long H., Chen A., Yang G., Li Y., Lu P. *Thin Sol. Films*, **517**, 5601 (2009).
14. Facchetti A., Annoni E., Beverina L., Morone M., Zhu P., Marks T.J., Pagani G.A. *Nat. Mater.*, **3**, 910 (2004).
15. Farmanfarmaei B., Rashidian Vaziri M.R., Hajiesmaeilbaigi F. *Quantum Electron.*, **44**, 1029 (2014) [*Kvantovaya Elektron.*, **44**, 1029 (2014)].
16. Rashid A.N., Erny C., Gunter P. *Advanc. Mater.*, **15**, 2024 (2003).
17. Jiang P., McFarland M.J. *J. Am. Chem. Soc.*, **126**, 13778 (2004).
18. Van Stryland E.W., Vanherzeele H., Woodall M.A., Soileau M., Smirl A.L., Guha S., Boggess T.F. *Opt. Eng.*, **24**, 244613 (1985).
19. Said A., Sheik-Bahae M., Hagan D.J., Wei T., Wang J., Young J., Van Stryland E.W. *JOSA B*, **9**, 405 (1992).
20. Van Stryland E.W., Woodall M., Vanherzeele H., Soileau M. *Opt. Lett.*, **10**, 490 (1985).
21. DeSalvo R., Said A.A., Hagan D.J., Van Stryland E.W., Sheik-Bahae M. *IEEE J. Quantum Electron.*, **32**, 1324 (1996).
22. Sarkar S., Guibal E., Quignard F., SenGupta A. *J. Nanopart. Res.*, **14**, 715 (2012).
23. Gupta S., Zhang Q., Emrick T., Balazs A.C., Russell T.P. *Nat. Mater.*, **5**, 229 (2006).
24. Rashidian Vaziri M.R. *Chinese Phys. B*, **24**, 114206 (2015).
25. Vaziri M.R. *Opt. Commun.*, **357**, 200 (2015).
26. Fakhri P., Vaziri M.R., Jaleh B., Shabestari N.P. *J. Opt.*, **18**, 015502 (2015).
27. Vijayalakshmi R., Rajendran V. *Arch. Appl. Sci. Res.*, **4**, 1183 (2012).
28. Manikandan K., Ahamed A., Thirugnanasundar A., Brahmanandhan G. *Dig. J. Nanomater. Biostruct.*, **10**, 1427 (2015).
29. Vaziri M.R., Omidvar A., Jaleh B., Shabestari N.P. *Opt. Mater.*, **64**, 413 (2017).
30. Omidvar A., RashidianVaziri M., Jaleh B., Shabestari N.P., Noroozi M. *Chinese Phys. B*, **25**, 118102 (2016).
31. Koole R., Groeneveld E., Vanmaekelbergh D., Meijerink A., de Mello Donegá C. *Nanoparticles* (Berlin, Heidelberg: Springer, 2014) pp 13–51.
32. Kelly K.L., Coronado E., Zhao L.L., Schatz G.C. *The Optical Properties of Metal Nanoparticles: the Influence of Size, Shape, and Dielectric Environment* (ACS Publications, 2003).
33. Umebayashi T., Yamaki T., Itoh H., Asai K. *Appl. Phys. Lett.*, **81**, 454 (2002).
34. Zhu W., Qiu X., Iancu V., Chen X.-Q., Pan H., Wang W., Dimitrijevic N.M., Rajh T., Meyer III H.M., Paranthaman M.P. *Phys. Rev. Lett.*, **103**, 226401 (2009).
35. Chen X., Liu L., Peter Y.Y., Mao S.S. *Science*, **331**, 746 (2011).
36. Zuo F., Wang L., Wu T., Zhang Z., Borchardt D., Feng P. *J. Am. Chem. Soc.*, **132**, 11856 (2010).
37. Wendt S., Sprunger P.T., Lira E., Madsen G.K., Li Z., Hansen J.O., Matthiesen J., Blekinge-Rasmussen A., Lægsgaard E., Hammer B. *Science*, **320**, 1755 (2008).
38. Li W., Ni C., Lin H., Huang C., Shah S.I. *J. Appl. Phys.*, **96**, 6663 (2004).
39. Spurr R.A., Myers H. *Analyt. Chem.*, **29**, 760 (1957).
40. Shiraishi Y., Hirakawa H., Togawa Y., Sugano Y., Ichikawa S., Hirai T. *ACS Catalysis*, **3**, 2318 (2013).
41. Marino E., Kodger T.E., Crisp R.W., Timmerman D., MacArthur K.E., Heggen M., Schall P. *Angew. Chem.*, **129**, 13983 (2017).
42. Sheik-Bahae M., Said A.A., Wei T.-H., Hagan D.J., Van Stryland E.W. *IEEE J. Quantum Electron.*, **26**, 760 (1990).
43. Vaziri M.R.R. *Appl. Opt.*, **52**, 4843 (2013).
44. Divya S., Nampoori V., Radhakrishnan P., Mujeeb A. *Chinese Phys. B*, **23**, 084203 (2014).
45. Divya S., Nampoori V., Radhakrishnan P., Mujeeb A. *Appl. Phys. A*, **114**, 1079 (2014).
46. RashidianVaziri M., Hajiesmaeilbaigi F., Maleki M. *J. Opt.*, **15**, 025201 (2013).
47. Vivas M., Shih T., Voss T., Mazur E., Mendonca C.R. *Opt. Express*, **18**, 9628 (2010).